Lab on a Chip

Constant-potential environment for activating and synchronizing cardiomyocytes colonies with on-chip ion-depleting perm-selective membranes

Journal:	*Lab on a Chip*
Manuscript ID	LC-ART-08-2020-000809.R1
Article Type:	Paper
Date Submitted by the Author:	01-Oct-2020
Complete List of Authors:	Yadav, Vivek; University of Notre Dame, Department of Aerospace and Mechanical Engineering Chong, Nicolas ; University of Notre Dame, Bioengineering Graduate Program Ellis, Bradley; University of Notre Dame, Bioengineering Graduate Program Ren, Xiang; University of Notre Dame, Department of Aerospace and Mechanical Engineering Senapati, Satyajyoti; University of Notre Dame, Department of Chemical and Biomolecular Engineering; University of Notre Dame, Center for Microfluidics and Medical Diagnostics Chang, Hsueh-Chia; University of Notre Dame, Dept of Chemical and Biomolecular Engineering Zorlutuna, Pinar; University of Notre Dame, Department of Aerospace and Mechanical Engineering

ARTICLE

Received 00th July 2020,

DOI: 10.1039/x0xx00000x

Constant-potential environment for activating and synchronizing cardiomyocytes colonies with on-chip ion-depleting perm-selective membranes†

Vivek Yadav[a, b], Nicholas Chong[cϕ], Bradley Ellis[cϕ], Xiang Ren[c], Satyajyoti Senapati[a, b, d], Hsueh-Chia Chang[a, b,c, d, *] and Pinar Zorlutuna[a,c,d,*]

In this study, an ion depleted zone created by an ion-selective membrane was used to impose a high and uniform constant extracellular potential over an entire ~1000-cell rat cardiomyocyte (rCM) colony on-a-chip to trigger synchronized voltage-gated ion channel activities while preserving cell viability, thus extending single-cell voltage-clamp ion channel studies to an entire normalized colony. Image analysis indicated that rCM beating was strengthened and accelerated (by a factor of ~2) within minutes of ion depletion and the duration of contraction and relaxation phases were significantly reduced. After the initial synchronization, the entire colony responds collectively to external potential changes such that beating over the entire colony can be activated or deactivated within 0.1 s. These newly observed collective dynamic responses, due to simultaneous ion channel activation/deactivation by a uniform constant-potential extracellular environment, suggest that perm-selective membrane modules on cell culture chips can facilitate studies of extracellular cardiac cell electrical communication and how ion-channel related pathologies affect cardiac cell synchronization. The future appications of this new technology can lead to better drug screening platforms for cardiotoxicity as well as platforms that can facilitate synchronized maturation of pluripotent stem cells into colonies with high electrical connectivity.

Introduction

Exogenous electric fields though underappreciated, find relevance for tissue engineering applications in circadian rhythm, cancer progression, wound healing, pluripotent stem cell maturation and regeneration[1–6]. Exogenous fields have been applied to electrically excitable cells such as cardiomyocytes to biomimic the *in vivo* environment[7]. Both Alternating (AC) and Direct (DC) Current stimulations have been shown to promote cardiomyocyte (CM) contraction in long term cultures that could otherwise show a decrease in contractile properties over time[8–10]. Additionally, various advanced microfluidic techniques have been utilized to apply electrical stimulations to heart-on-chip platforms for cardiotherapeutic drug screening studies, disease modeling, and monitoring of CMs contractile properties[11–13]. AC field is commonly used in cardiac development, defibrillation and pacing cells to a desired physiological frequency[14]. AC field has also been used to mature pluripotent stem cells into cardiomyocytes[6,15]. The exogenous fields typically have low amplitude (1-6 V/cm), low frequency (0.1-6Hz), with (0.25-10ms) monophasic/biphasic square/sinusoidal pulse waveform[16]. Short-duration (~ms) but high power AC field has also been shown to successfully treat cardiac dysrhythmias[17]. Although the threshold for defibrillation is around (6-36 V/cm), a much higher field is required to counter the signal loss in the skin. Unfortunately, electric fields beyond 50V/cm lead to irreversible and potentially lethal cellular damage[18–20]. Additionally, both DC and AC currents that exceed ~3mA lead to harmful Faradaic products, pH changes, and high Joule heating (~tens mW) causing additional cell death along with undesirable air bubble formation in microchannels[7,19–21]. Also, typical cell culture medium has a homogenous electrolyte distribution and a potential gradient (field) that drives an ionic current through the medium. Consequently, each cell sees a different potential in its extracellular environment. Moreover, since the extracellular medium is much more conducting than the cell membrane, very little field penetrates the cell membrane and most field lines circumvent the cells altogether. The induced voltage drop across most cells in the earlier experiments with external fields is hence less than the approximately 20mV - 50mV required to activate or deactivate ion channels. Consequently, even though many of the studied

[a] Department of Chemical and Biomolecular Engineering, University of Notre Dame, Notre Dame, IN 46556, USA
[b] Center for Microfluidics and Medical Diagnostics, University of Notre Dame, Notre Dame, IN 46556, USA
[c] Department of Aerospace and Mechanical Engineering, University of Notre Dame, Notre Dame, IN 46556, USA
[d] Harper Cancer Research Institute, University of Notre Dame, Notre Dame, IN 46556, USA

*Corresponding authors: hchang@nd.edu, Pinar.Zorlutuna.1@nd.edu
ϕ Equal contribution
† Electronic Supplementary Information (ESI) available: See DOI: 10.1039/x0xx00000x

phenomena (including various pathologies) are related to how voltage-gated ion channel activities affect the entire colony, actual studies of how a cell colony responds collectively to induced voltage across the membrane of each cell by an external field is under studied[22]. In contrast, there is a huge body of voltage clamp studies of how cross-channel voltage changes the ion-channel conductance of a single cell, in the absence of any intercellular electrical communication or even single-cell autonomous action potential dynamics[23–30]. Additionally, a large focus for cardiotoxicity testing in drug development has been in the automation of this technology for high throughput drug discovery[28,30-33]. Unfortunately, these developments in addition to testing on single cells, also only test a single ion channel, the human Ether-a-go-go-Related Gene (hERG) and are inadequate in completely ruling out potentially toxic compounds prior to costly and time intensive dog telemetry studies[34] .Both the single ion channel and single-cell deficiencies of the voltage-clamp technique hence prevents in-depth study of how voltage-gated ion-channel pathologies and drugs are connected to dynamic intercellular communication in a multicellular culture. While external electrodes and external electrode arrays can influence and pace the cells, they cannot sustain a constant potential over the entire colony so that the ion-channel activities of the entire synchronized colony can be studied.

In this report, we introduce a novel non-invasive, flow-free and user-friendly technique to generate a high, uniform potential in the extracellular environment of an entire rCM colony by isolating the colony with low conductivity solutions. The steady-state and high-gradient ion concentration profile of low conductivity buffer is imposed without external reservoirs and is sustained indefinitely by the ion-depletion action of a perm-selective membrane. Such steady concentration gradient is otherwise difficult as the diffusion time is on the order of minutes for the dimension of a typical chip. Electric fields applied at the two ends of the ion-depletion zone enter and exit the high-conductivity colony without Joule heating or a significant current and the colony maintained a constant (tunable) voltage. The polarity of the extracellular voltage at the colony can also be changed, if the perm-selective membrane is replaced by one with opposite selectivity. In the current report, we only apply a positive extracellular voltage with a cation exchange membrane (CEM). Instead of using Nafion or other monolithic membranes synthesized in situ[35-37], we cut pieces from commercial desalination membranes and assemble them into our chips. We have previously used such low-cost membrane-based microfluidic devices to induce depletion action for pH actuation, analyte concentration/isolation and molecular sensing[38-41]. The electric field in the depleted region is as high as 100V/cm, higher than any previously published DC or AC exogenous fields, but with a relatively low current (~100s μA, ~sub mW) to minimize Joule heating. This novel synchronization technique demonstrates significant usability not only in its ability to rapidly synchronize entire cardiac colonies demonstrated in this study, but also potentially in the fields of drug development to bridge the gap between high throughput hERG voltage-clamp studies and low throughput costly dog telemtry studies. Additionally, this technique can provide useful insight in cardiac development and human induced pluripotent stem cell (hiPSC) derived cardiomyocyte (iCM) and neuron maturation.

Materials and Methods:

Microfluidics and device fabrication:

Wax mold printing

The mold was designed in SolidWorks 2017 software (Dassault Systemes SolidWorks Corporation, USA) and was transferred as an STL (stereo-lithography) file to a wax 3D printer (Solidscape Studio-Solidscape, Inc.). A sacrificial layer (Melt/Dissolvable wax (Solidscape, Inc)) was made around the main structure (Midas Castable Material (Solidscape Inc., USA)) to prevent mold breakage during post processing. Once the print job is completed, the print bed is removed from the printer and placed on top of a hotplate for 1 hour at 75°C to loosen the wax mold for subsequent detachment. The sacrificial wax layer was then dissolved in BIOACT VSO (Vantage Specialty Chemicals) solvent for 2 days. When the sacrificial layer is fully dissolved, the devices are removed from the solvent and carefully wiped clean with narrow fiber paint brushes. They are then immersed in USP grade white mineral oil for the removal of trace amounts of VSO, and then rigorously air dried with an air blower.

PDMS device fabrication

A 1:10 weight ratio of curing agent and polydimethylsiloxane (PDMS, Sylgard 184, Dow Corning) base was mixed thoroughly and then degassed for 30 minutes to remove air bubbles. PDMS was then poured into the previously described molds and degassed again to remove any trapped air bubbles, followed by overnight curing at 35°C. After curing, the wax print was removed by washing with dimethyl sulfoxide (manufacturer) (DMSO) for 3 hours to completely dissolve the wax mold. To remove the DMSO residual on the PDMS, isopropanol (IPA) was sprayed onto the PDMS. The DMSO was then thoroughly removed and a 1mm biopsy punch was used to punch inlets and outlets. Both the device surface and 25x75mm glass slides (Ted Pella, USA) were rinsed with IPA, dried, and then placed into a plasma cleaner (Harrick-Plasma PDC-001,USA) for 2 minutes for air plasma treatment. Following air plasma treatment, devices were bonded together and incubated overnight at 80°C.

Neonatal rat cardiomyocyte isolation

Animal studies were approved by the Institutional Animal Care and Use Committee at the University of Notre Dame. The animal procedures conformed to the NIH Guide for the Care and Use of Laboratory Animals. Neonatal rCMs were isolated from 2 day old rats (Sprague-Dawley, Charles River Laboratories) using a previously established protocol[42]. Briefly, the pups were anesthetized with isoflurane followed by immediate decapitation and excision of the heart. The hearts were then digested and ventricular cardiomyocytes were isolated and seeded into the microfluidic device as described.

Device seeding

Prior to rCMs isolation, devices were washed with PBS (VWR, USA) and sterilized under UV light for 30 minutes. Devices were then incubated with fibronectin (50 µg/mL) (Sigma Aldrich, USA) for 30 minutes at 37˚C. After incubation, custom made PDMS blockers were inserted into the two large reservoirs and outlets in the depletion channel to localize rCM attachment to the seeding channel. Following blocker placement, the devices were washed with fresh, filtered DMEM supplemented with FBS (10%) (Hyclone, USA) and penicillin (1%) (Sigma Aldrich, USA). Finally, devices were placed in a petri disch containing 1.5mL of PBS supplemented with penicillin (5%) and stored until seeding.

Following rCM isolation, 20µl of the cell suspension (~150,000 cells) were seeded into each device. Devices were then cultured overnight under normal incubation conditions (37˚C, 21% O_2, 5% CO_2) to allow for cell attachment. The next day, cell attachment was confirmed and the media was changed to remove any cell debris and/or dead cells remaining in the device. Devices were then imaged using a Zeiss Axiovert 200M Fluorescence/Live cell imaging inverted microscope.

Voltage measurement

In order to perform voltage measurements within the microfluidic device, a new 3D printed mold was designed and manufactured as described above. Two different aluminum wires were attached to the junction of seeding and depletion channel respectively to measure the voltage drop across the ends of the connecting channel. To perform voltage measurement tests, the wires coming from the two ends were connecting to a digital multimeter (34401A Agilent Multimeter, USA). The data was recorded using BenchVue software (Keysight Technologies, USA).

Experimentation:

Electrical stimulation

CEMs with negative charge due to organosulfanate groups were procured from Mega a.s. (Czech Republic). Membrane reservoir fabrication was performed as described previously[43]. Briefly, a small piece of CEM (~$10\ mm^2$) was embedded in a two component fast curing resin (TAP Plastic Inc., USA) in 1:1 ratio for 30 minutes in a custom designed mold in a two component silicon RTV system (TAP Plastic Inc.). After releasing the mold, a hollow cylindrical structure with an exposed CEM surface was obtained. The membrane was kept in a microcentrifuge tube (Argos Technologies, USA) filled with Phosphate Buffer Saline (PBS) (Fisher Scientific, USA) for overnight swelling followed by overnight UV sterilization. While performing experiments, the membrane reservoir was gently pushed inside the PDMS device seeded with rCMs. For the other reservoir, 1000 µl pipette tips (VWR, USA) were cut with a razor blade and were gently pushed to create a seal with the PDMS and filled with cell media. The cell media was then subsequently changed to remove any trapped bubble during the process and was kept under normal cell culture conditions for 30 minutes. The device was then placed in a sterilized Zeiss Stage Incubator, under standard culture conditions and incubated for 20 minutes to achieve synchronous beating. For stimulation tests with the CEM, two platinum electrodes were inserted into the device, with the negative electrode placed in the membrane reservoir and the positive in the open reservoir. For no membrane studies, the two open reservoirs were filled with cell media and electrodes were placed in them. Voltage was then applied using a DC power supply (Biorad PowerPac Basic Electrophoresis Power Supply, USA) and current was observed using a digital multimeter (34401A Agilent Multimeter, USA). A voltage of 45V was chosen and is applied throughout the paper unless otherwise mentioned. All videos were recorded at 30 fps.

Video analysis

The video files were converted from ZEN files to .avi, which are subsequently analyzed via a custom written image analysis code in Matlab based on previously published algorithms[7,44]. The approach is based on the analysis of the change in pixel intensity in a bright field video over time with respect to its subsequent frame. Parameters for illumination for optical microscopy were optimized before taking a video. Fig. 1(e) shows a representative trace of rCMs contraction extracted from image analysis. The raw trace was normalized to its mean value during the analysis time interval. The obtained time series was then further analyzed to obtain various time scale parameters such as peak to peak time, contraction time (CT), Relaxation Time (RT), Contraction-Relaxation Duration (CRD), number of peaks, normalized Maximum Contraction Speed (MCS) and normalized Maximum Relaxation Speed (MRS). The beating frequency was calculated by dividing the obtained number of contraction peaks by the duration of the observation period. Each experimental trace of beating frequency was normalized to its initial 10s value to quantitatively represent the progression of beating frequency in each experiment. The onset of contraction denotes the time point the intensity is 10% above its difference from the peak amplitude and its baseline value. The CT is then calculated as the difference between the onset time till the velocity becomes minimum. The RT is also calculated in a similar fashion. The end of relaxation is marked as the 90% reduction in its amplitude value with respect to its baseline value. The CRD was then calculated by summing both the CT and RT. “Image correlated field potential duration” was defined as the time interval between the onset of contraction to the peak of relaxation motion.

Immunohistochemistry

Standard immunohistochemistry staining was performed. Briefly, rCMs were fixed with 4% paraformaldehyde (Electron Microscopy Sciences, USA) for 30 minutes followed by permeabilization with 0.1% Triton-X (Thermo Fisher Scientific, USA) for 15 minutes. Samples were then blocked and then incubated with cardiac troponin t (Abcam, USA) and HCN2 (Abcam, USA) primary antibodies overnight at 4°C. After primary antibody incubation, samples were then incubated with secondary antibody for 6 hours at 4°C followed by DAPI staining for 10 minutes at room temperature. Samples were then imaged with a Zeiss Axio Observer.Z1 fluorescence microscope and processed with Zeiss Zen software.

Statistical analysis

The data in this study has been presented as Mean ± Standard Error of the Mean (S.E.M) unless otherwise specified. For box and whisker plots, the whiskers represent the SEM. The obtained data was compared with either a two sample t test or, for experiments with more than two sample groups, a one-way ANOVA with Tukey's post hoc test was performed and the value of $p<0.05$ was considered significant.

Results and discussions:

Figure 1 shows the overall device design and predicted and measured voltage drops at distinct regions of the device. We deplete the ions in the straight channel shown in Fig. 1(a). The cells are seeded in a parallel channel and are connected to the first depletion channel by a side channel. This field potential is still lower than the threshold field required to damage molecules such as DNA or proteins present within the cell culture and media (tens of kV/cm)[45]. Because of the electrode placement, our simulation of the leaky dielectric model of electrolytes in Fig. 1(b) shows that depletion occurs only in the depletion channel. The field is negligible in the cross channel and the cell colony sees a uniform potential that can be controlled via the applied voltage.

The depletion channel contains a CEM embedded in polyurethane resin and a reservoir for applying voltage. All the experiments were performed by generating a depletion front in the depletion channel whereas ion enrichment experiments caused the current in the circuit to rise past 3mA resulting in cell death. Fig. 1(c) demonstrates the extent of depletion through the use of a charged fluorescence dye solution. It is shown to extend slightly into the connecting side channel but not into the cell channel, as is consistent with our simulation. Fig. 1(d) represents the bright field image of the region of interest, at the junction between the side and cell channel. Fig. 1(e) is a schematic of the time series obtained from image analysis described in detail in the experimentation and video analysis sections.

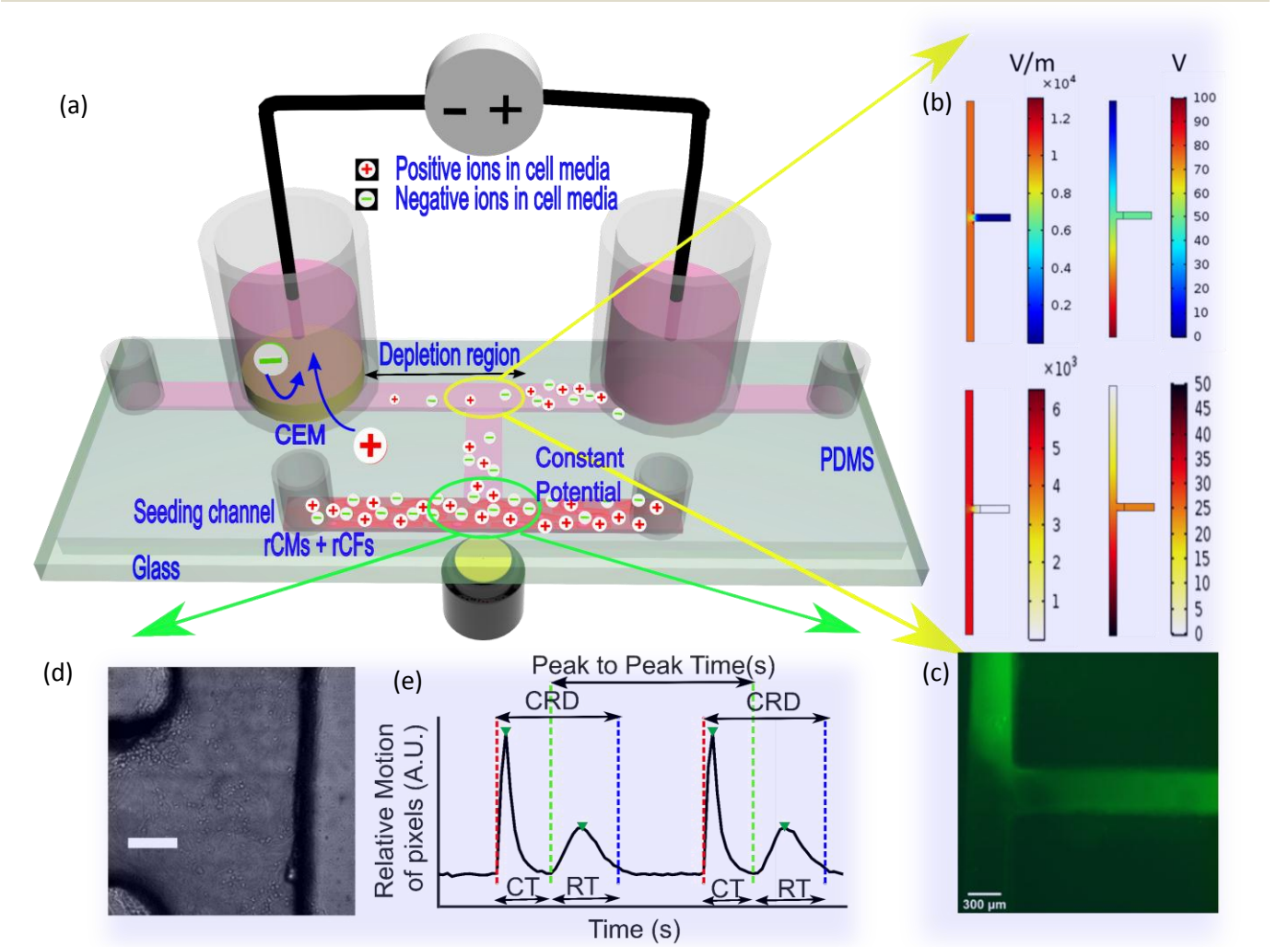

Figure 1: Overview of the experimental platform (a) Schematic representation of the experimental setup (b) Finite element simulation results of field and potential in the zoomed section showing a uniform potential in the cell colony (c) A picture of the chip showing location of the depletion front developed by the applied field. A negatively charged Fluorescein dye is used to track the depletion front. Scale bar represents 300µm (d) A bright field image of the region where rCMs are seeded (Scale bar is 100µm) and (e) a representative trace obtained by image analysis and time series analysis.

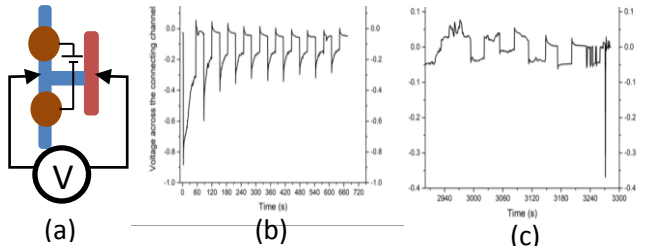

Figure 2: Voltage drop measurement across the connecting channel. (a) Schematics of voltage measurement setup and observed voltage change across the side channel with (b) and without (c) a CEM

The beating motion of rCMs in a small neighborhood was observed via timelapse imaging (see Supplementary Video 1 in Supplementary Materials: DOI: 10.1039/ x0xx00000x). The rCMs exhibit first a contraction peak followed by a relaxation peak and then a long stationary transient is observed before the twin peaks appear again. As shown by Hayakawa et al[46], the contraction phase is related to the depolarized plateau phase and the relaxation phase occurs during the hyperpolarization phase (see Fig. S1 in Supplementary Materials: DOI: 10.1039/ x0xx00000x). To facilitate fabrication of the required multilayer structure design, 3D-printed meltable wax mold was used to fabricate smooth 300 µm wide channels. Fig. S3 (Supplementary Materials: DOI: 10.1039/ x0xx00000x) shows the fabrication process which is described in detail in microfluidics device fabrication section.

To demonstrate that the cell channel is under a uniform potential, we measure the voltage drop across the connecting side channel in two chips as shown in Fig. 2(a), one with and the other without the CEM membrane. Fig. 2 (b) and Fig. 2(c) depicts the measured voltage in response to irregular 'ON' and 'OFF' switching of the voltage. With the CEM membrane, a characteristic RC transient after voltage activation leads to a constant voltage drop. Without the membrane, a constant potential is never reached in the cell colony. Instead, rapid fluctuations are observed, quite possibly due to microbubble formation and Faradaic reactions, which are expected beyond 10V[47]. Depletion action by the CEM has hence eliminated such fluctuations and produced a constant potential in the cell channel.

Effect of voltage on rCM beating dynamics

`Fig. 3 demonstrates the effect of the uniform potential microenvironment on beating rCMs during the first five minutes of application through CEM. The rCMs start responding to the elevated extracellular potential instantaneously. This is evident from the normalized contraction-relaxation trace obtained from image analysis as presented in Fig. 3(a) showing a discernable difference in the time series before and immediately during the application of voltage. Some reduction in the width of both the contraction and relaxation peaks is also evident. In order to better visualize the transient, the normalized beating frequencies were calculated after every 10s and plotted against time as shown in Fig. 3(b). For initial 30s no voltage was applied, and the voltage was turned on subsequently after that for the rest of the five-minute recordings. Under the influence of the applied external field, the beating frequency increased and then saturates at around 3 minutes for the stimulated cases. The beating frequency remained roughly stable for the next two minutes at a higher beat rate than

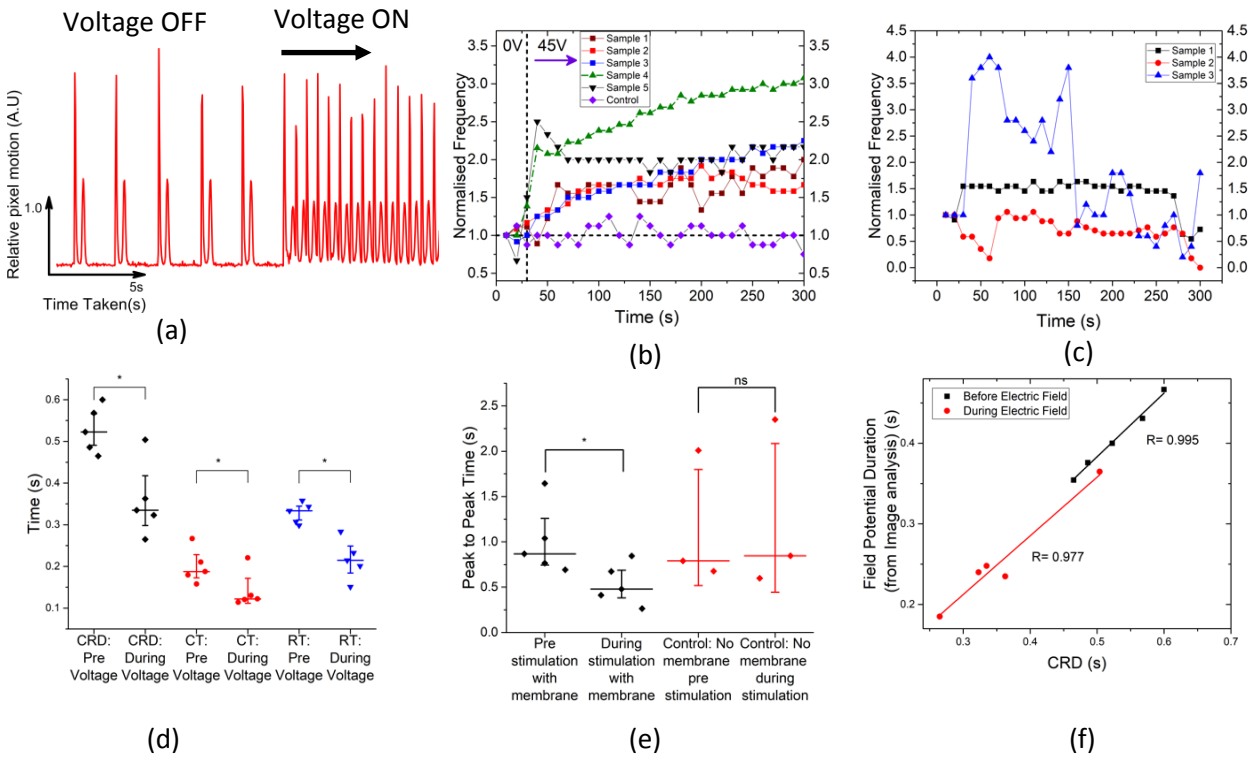

Figure 3: Effect of voltage on the time scales of uniformly beating rCMs with and without CEM during first five minutes of the depletion (a) The trace evaluated from image analysis depicting the abrupt transition when voltage is turned on (b) The beating frequency transient. The beating frequency is normalised by dividing the frequency obtained in each 10s interval with its initial 10s value (n=5) (c) The beating frequency transient in the control study without using a membrane (n=3) (c) The comparison of total time taken to complete an oscillation, CT and RT scales before applying voltage (0-30s) and during the application of voltage (210-240s) for a 30s time interval in all cases (*p <0.05) (e) The peak to peak time before and during the electrical stimulation (*p <0.05) (f) Correlated Field potential duration (onset of contraction to relaxation peak) obtained from Image analysis vs the total contraction-relaxation time CRD taken for a beat indicates contraction initiation dynamics is reduced in duration in proportion to the full contraction duration .

the original beating frequency (2.23± 0.52-fold change compared to baseline). The control transient trace shown in Fig 3(c) represents the un-stimulated control sample when no voltage was applied to the setup and approximately maintained its original value till the end of the five-minute recording window. Most striking is the separation of the contraction/relaxation twin peaks reduces significantly as seen in Fig. 3(d).

To explore the effect of spatial uniformity of the extracellular potential introduced by the depletion action of the CEM, a voltage was applied without using CEM. A potential of 45V was unsuccessful as Joule heating caused permanent damage to the cells within five minutes of field induction. In order to perform a control study without CEM, the device was operated at a constant current. The current through CEM saturates in the range of 0.1 mA - 0.7 mA during the first five minutes and a higher end current, i.e. 0.7 mA was used for the control study as shown in Fig. 3(c). In these experiments without CEM, synchronized beating was not observed and the beating profile of the cells was unstable and irregular. The beating frequency in two of the no membrane control studies decreased below its initial value till the end of five-minute time period while it was highly unstable in the other one as shown in Fig. 3(e). This "counter example" highlights the effect of non-uniform potential. Without the depletion, the potential varies significantly across the cell colony and synchronization becomes impossible.

Since the beating rate stabilizes within the first three minutes of voltage being applied, the beating dynamics can be contrasted to better understand the effect of a high extracellular potential on the rCMs. An arbitrary 30s time interval (210 - 240s) was chosen when the beat rate was stable and contrasted against the first 30s when no electric field was applied. As shown in Fig. 3(d), the RT and CT both decrease appreciably compared to when no field was applied. In Fig 3(e), the significant difference in the peak-to-peak CRD duration of the cells at equilibrium in the polarized phase is also apparent in Fig. 3(a). These effects were not observed without the CEM. To establish the depolarization cycle is self-similar, the image correlated applied potential duration between the onset of

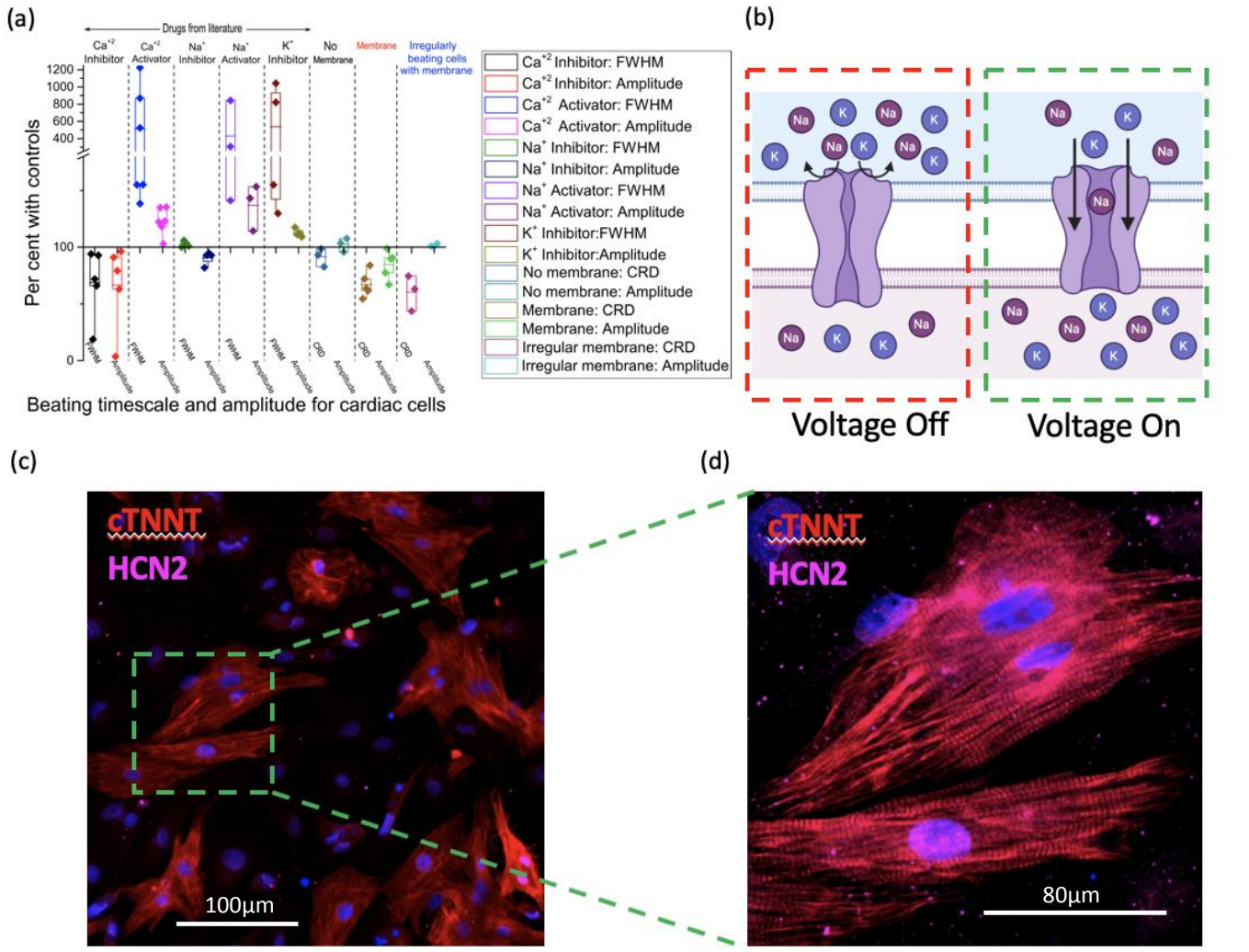

Figure 4: (a) Comparison of cardiomyocytes motion kinetics with literature (ref 46,55,59-61) depicting the effect of voltage gated ion channel agonists/antagonists.[FWHM (Full width at half maximum), roughly corresponding to the CRD peak-to-peak time between contraction and relaxation, is from the trace obtained by using Calcium dye (Fluo-4) and CRD is the Contraction-Relaxation time obtained from bright field video analysis. (b) Cartoon schematic of an rCM HCN2 channel with the voltage turned off (closed) and on (open). (c and d) rCMs stained for cardiac troponin t (cTTNT, red) and HCN2 (magenta).

contraction to the relaxation peak was plotted against the CRD between peaks in Fig. 3(f) and a good linear and near-identical correlation was observed during the "off" (R=0.995) and "on" (R=0.977) states. This suggests that the entire depolarized phase is reduced in duration due to voltage-gated activities.

We are able to form hypothesis on ion-channel mechanisms from the dynamics triggered by uniform constant potential. From voltage clamp experiments, a positive extracellular potential (or a negative intracellular potential) is known to activate HCN ion channels and deactivate all other Calcium, Sodium and Potassium channels, for cardiomyocytes Fig. 4(a)[48–54]. In prior voltage clamp and drug activation/inhibition experiments on voltage-gated ion channel conductance, the duration of the long polarized interval between the twin contraction/relaxation peaks, when the cell is in equilibrium and motionless, is reduced by activating HCN ion channels to trigger depolarization sooner and the width of the depolarized plateau is shortened by deactivating L-type Ca_v ion channels which sustain a positive membrane potential[46,55–58]. Our observation that the peak-to-peak time is reduced by a factor of two and the contraction and relaxation intervals are also reduced is consistent with activated HCN and deactivated L-type Ca_v channels by a positive extracellular potential. This suggests that these channels may be more sensitive to a positive external potential than other cardiac related ion channels.

As HCN channel is the only channel that is activated by a positive external potential based on the literature from single-cell voltage clamp experiments, and it might be chiefly responsible for the duration of the polarized phase with negative membrane potential[57,58], we suggest that these observations are at least partially due to activation of the HCN2 channels Fig. 4(b). In this study, we confirmed the existence of HCN2 channels in our neonatal rCM cells in Fig. 4 (c and d) via immunostaining. In future studies, we will look to further confirm this observation with drug-activated HCN studies.

We are able to confirm that drug-deactivated Ca_v ion channels reduce the peak-to-peak contraction and relaxation CRD durations and amplitudes during the depolarized phase with respect to controls by analyzing existing literature[46,55,59-61] as presented in Fig. 4(a). No other drug activated or deactivated ion channels examined in the literature show this particular feature. The ~~amount of~~ reduction in both CRD duration and amplitude of these two peaks is comparable to our data qualitatively. This suggests that we can mimic drug deactivation of Ca_v ion channels with our uniform positive potential on the entire rCM colony. This timescale of milliseconds is a much more rapid assay than drug induced studies which typically induce a response on the scale of seconds to minutes. It is to be noted that the data taken from literature shown in Fig 4(a) has high variability and experiments were performed in different devices. However, we have utilized them to solely develop a qualitative estimate of rCM behavior. Completely testing of the hypothesis requires very extensive and detailed experimentation which is beyond the scope of the current manuscript. These suggested mechanisms are proof-of-concept studies to show the

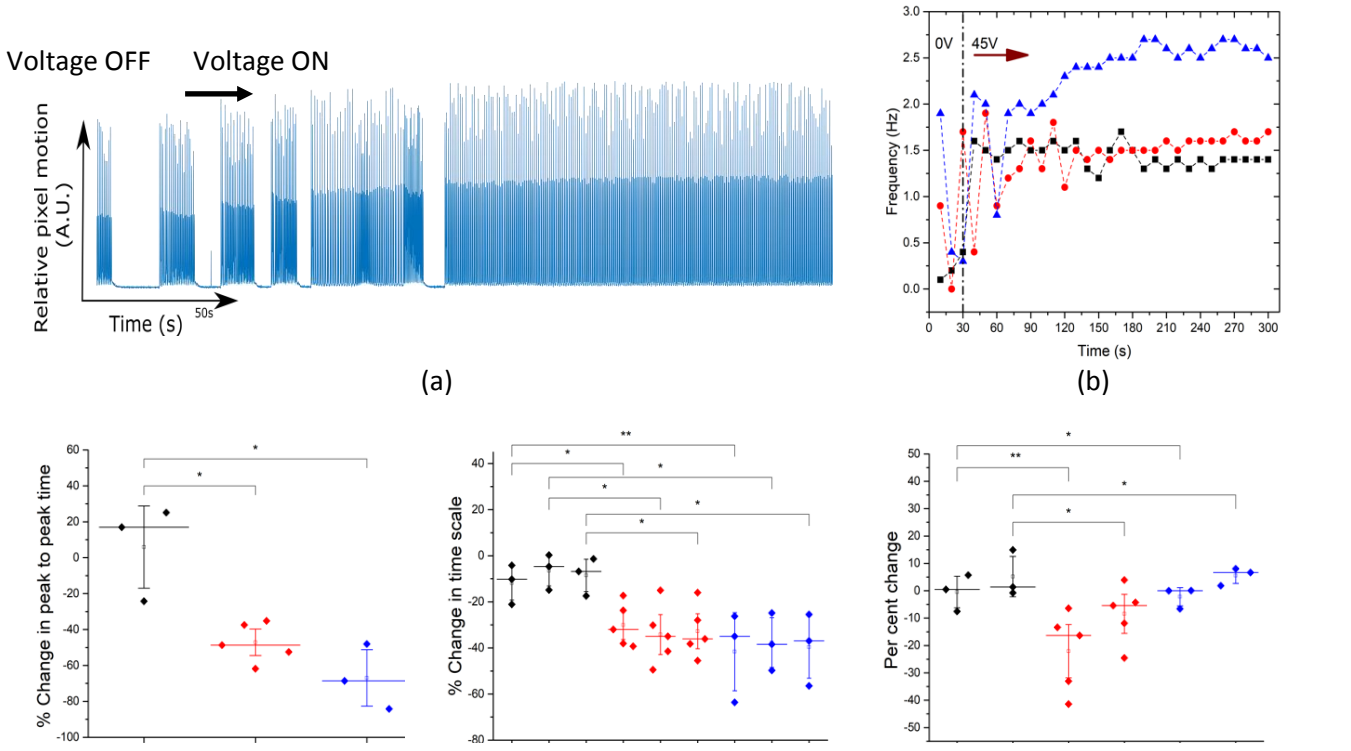

Figure 5: Irregularly beating cells with regular beats during electrical stimulation and comparative studies (a) Trace of the entire event. Depicting sporadic beats which stabilized within minutes after the application of voltage. (b) The beating frequency transient depicting the rCMs were beating intermittently. Application of voltage after the 30s of recording showed that they stabilized and saturated to at an elevated beating frequency. (c) The percentage change in peak to peak time before and during the experiment between the no membrane control, membrane and irregularly beating cells with the membrane. Two sample t test was performed (*p<0.05) (d) The percentage change in CT, RT and contraction relaxation duration before and during the experiment between the no membrane control, membrane and irregularly beating cells with the membrane. Two sample t test was performed (*p<0.05, **p<0.1) (e) The percentage change in maximum contraction speed and maximum relaxation speed: before and during the experiment between the no membrane control, membrane and irregularly beating cells with the membrane. Two sample t test was performed (*p<0.1, **p=0.556).

usefulness of our technology.

Effect of uniform potential in colony synchronization

Our data also suggest that we are enhancing rCM synchronization with the applied uniform extracellular potential, which would be consistent with potential activation of the HCN ion channels. Our first observation on synchronization was seen during the first five minutes of voltage induction: application of voltage using CEM synchronized the beating rate of otherwise irregularly beating rCMs clusters into a single frequency. These rCM clusters were beating sporadically and stopped intermittently. When they did beat, there was local synchrony but not throughout the entire colony. The contraction-relaxation trace obtained from image analysis for the entire recorded time period of one such case is displayed in Fig. 5(a) where the irregularly beating cells are stabilized by the uniform potential during the first recorded five minutes. The corresponding beat rate is displayed in Fig 5(b) where the beating frequency was highly irregular before applying voltage. Turning on the voltage stabilized the beating frequency roughly during the first three recorded minutes. For comparison, the percentage change in the time scales in the 30 seconds interval before applying voltage and 30 seconds (210-240s) afterwards was calculated for all the cases: voltage without membrane, voltage with membrane and voltage with membrane on irregularly beating cells in Fig. 5 (c and d). Fig. 5(e) shows significant percentage change in the peak to peak time was observed between the cases when ion exchange membrane was present as compared to the one without it. The CT and RT time scales also showed a significant difference between the no-membrane cases as compared with the cases presented with the membrane. The percentage change in beat velocities for both relaxation and contraction were not significant for the cases with electrical stimulation with membrane as compared to the control samples without membrane. It is hence quite clear that the uniform potential introduced by the depletion action of the CEM significantly increases synchronization over the entire colony. As demonstrated in Figure 4 c and d, both the isotropic and non-uniform nature of the rCMs potentially hinder the synchronization efficiency of the constant-potential environment created using the ion depletion technology. There is extensive evidence in literature that an anisotropic environment promotes

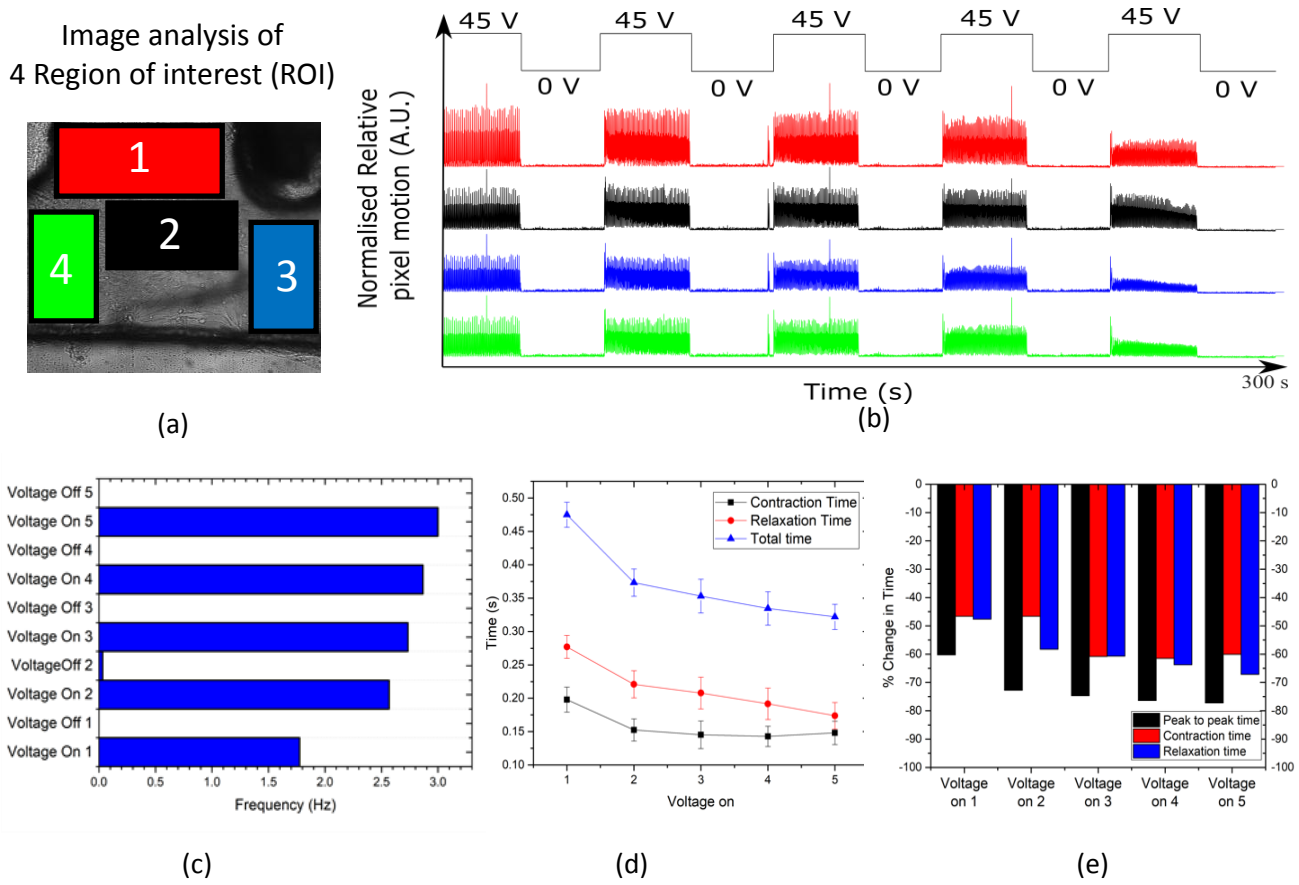

Figure 6: On command synchronization of cardiomyocytes with the applied voltage pulse (a) A snapshot of the image of the cells at the junction of the connecting channel and the cell channel. Four different spatial Region of Interest (ROI) were identified for subsequent image analysis. (b) The trace obtained from 4 ROI and their behaviour with ON/OFF applied field (c) The beating frequency each time when the voltage is switched ON and OFF. (d) The contraction (CT), relaxation (RT) and total (CRD) time to complete a beat during the time when the voltage in ON. Error bars are the standard deviation for the respective time scale (e) The percentage change in the relaxation, contraction and total time with respect to its pre-recorded value for each time when the voltage is switched ON.

enhanced electrical signaling and subsequent cardiomyocyte maturation both in rCMs and iCMs[62-69]. In a similar manner, the non-uniform nature of the rCM culture due to the inclusion (and subsequent proliferation) of cardiac fibroblasts which have been shown to significantly alter, and when present in larger quantities, potentially decrease signal propagation[70-73]. An increase in the rCM : fibroblast ratio could rectify this, as the inability of fibroblasts to trigger their own action potential and their propensity to dampen any signal passed through due to their internal resistance could potentially decrease ion movement between rCM clusters in the culture. Future studies will focus on these factors and the role they play both on the developed system itself, and in cardiomyocyte maturation.

hiPSCs have over the past decade established themselves as a promising cell resource for the study of human cardiac development and disease. Unfortunately, their use is hindered by issues regarding cell maturity and differentiation efficiency that prevent results directly mimicking what is seen clinically[14,74-78]. Long term AC stimulation of iCMs has shown promise as both a maturation and differentiation technique but have proven inadequate in definitively maturing iCMs to an adult phenotype[11,14]. The stimulation method developed in our study demonstrates for the first time, to our knowledge, the effect of DC electric field on cardiomyocyte autonomous synchronization. This rapid synchronization technique demonstrates great promise to enable novel studies to better promote iCM differentiation efficiency, maturation, and synchronization that will be further investigated in future studies.

On demand switching of synchronized beating with uniform potential

We observed an interesting event when the voltage was continuously applied to the rCMs in the microfluidic chip. As the depletion front approaches the junction of the depletion channel, localized change in the ionic strength occurs. In order to check the synchronous behavior of the cells and their spatial variations, four different spatial regions were identified as shown in Fig. 6(a). A binary mask was generated for each of these regions of interests and subsequent image analysis was performed on them one at a time. The trace obtained from image analysis from each of these four spatial locations is shown in Fig 6(b). The trace profiles reveal that the cells were beating 'on command' with the applied voltage. No phase difference or delay in the onset of contraction and relaxation was observed. As shown in Fig. 6(b), the 30s time period of square pulse voltage was applied five times. Every time rCMs responded to the applied electric field and stopped and started beating synchronously. As shown in Fig. 6(c), when the voltage was on at 45V, rCMs were beating synchronously and smoothly. When the voltage is turned off after 30s, the entire cluster stopped beating, with beating resuming at a higher frequency when the electric field was turned back on. The CT and RT show a decrease in their absolute values when the applied potential was switched on as evident from Fig. 6(d). The percent change was calculated in the peak-to-peak time scale, CT and RT with respect to the case when no voltage was applied to it. 70% reduction in peak-to-peak time was observed while for other time scales (contraction and relaxation) more than 50% reduction was observed as shown in Fig. 6(e).

A constant high DC potential in an extracellular environment to activate ion channels synchronously over the entire colony can offer invaluable insight into the electric coupling of neuron and cardiac cells. In neuron communication, extracellular charge generation due to ion channel fluxes have long been speculated to produce extracellular potentials that are far stronger than the action potential of a single neuron. This extracellular charge and potential has been hypothesized to be responsible for long-range synchronization of neuron cells by a mechanism termed "ephaptic coupling"[79]. A strong cloud of extracellular charge, released by a localized subset of synchronized cells, can produce far-reaching fields to recruit other cells to fire their ion channels synchronously. Long-range synchronization of cerebellar Purkinje cells, for example, has been attributed to this external field mechanism[80]. These observations demonstrates that potentially, neighboring cell communication can differ from global synchronization, with disparate time scales and potential amplitudes. It has yet to be established, to our knowledge, if such an external Ephaptic coupling mechanism exists within the heart and its potential relevance to the cardiovascular physiology. The on-chip system developed in this study will enable such new mechanisms to be studied for cardiac tissue and beyond.

Conclusions

In conclusion, we have used a permselective membrane on a chip to produce a uniform potential over an entire colony of rCMs, such that each cell in the colony sees the same elevated extracellular potential. From image and time series analysis, we see evidence that the uniformly applied external potential potentially synchronously deactivates L-type Ca^{2+} and activates HCN voltage gated ion channels. The former effect produces a similar reduction in the contraction and relaxation durations as drug-deactivation studies. Three novel synchronization phenomena were observed: a rapid on command synchronization of rCMs with the applied external potential, the ability to reversibly stop rCMs from contracting completely, and the ability to normalize irregular beating frequencies. Enabling voltage-gated channel activities synchronously over the entire communicating colony, without the use of voltage clamps, could allow better characterization of ion channel related pathology and drug effects on cell communication and synchronization, bridging the gap between the high throughput, but relatively narrow automated voltage clamp technologies and high cost, time intensive dog telemetry studies. We believe that such collective feedback induced by the constant potential microenvironment should also be invaluable in training pluripotent stem cells into cardiomyocytes or neuronal colonies with high connectivity.

Acknowledgement

The present work is supported by National Science Foundation (NSF) ECCS-1807551, Semiconductor Research Corporation (SRC) GRC TASK 2840.001, and the Naughton Fellowship.

Conflicts of interest

There are no conflicts of interest to declare.

References

1 L. P. da Silva, S. C. Kundu, R. L. Reis and V. M. Correlo, *Trends in Biotechnology*, 2020, **38**, 24–49.
2 J. Hunckler and A. de Mel, *J Multidiscip Healthc*, 2017, **10**, 179–194.
3 R. Wever, *Int J Biometeorol*, 1973, **17**, 227–232.
4 K. M. C. Oliveira, J. H. Barker, E. Berezikov, L. Pindur, S. Kynigopoulos, M. Eischen-Loges, Z. Han, M. B. Bhavsar, D. Henrich and L. Leppik, *Scientific Reports*, 2019, **9**, 11433.
5 A. Gothelf, L. M. Mir and J. Gehl, *Cancer Treatment Reviews*, 2003, **29**, 371–387.
6 S. S. Nunes, J. W. Miklas, J. Liu, R. Aschar-sobbi, Y. Xiao, B. Zhang, J. Jiang, S. Massé, M. Gagliardi, A. Hsieh, N. Thavandiran, M. A. Laflamme, K. Nanthakumar, G. J. Gross, P. H. Backx, G. Keller and M. Radisic, *Nature Methods*, 2013, **10**, 781–787.
7 N. Tandon, C. Cannizzaro, P. H. G. Chao, R. Maidhof, A. Marsano, H. T. H. Au, M. Radisic and G. Vunjak-Novakovic, *Nature Protocols*, 2009, **4**, 155–173.
8 E. Holt, P. K. Lunde, O. M. Sejersted and G. Christensen, *Basic Res Cardiol*, 1997, **92**, 289–298.
9 A. Grosberg, P. W. Alford, M. L. McCain and K. Kit Parker, *Lab on a Chip*, 2011, **11**, 4165–4173.
10 H. J. Berger, S. K. Prasad, A. J. Davidoff, D. Pimental, O. Ellingsen, J. D. Marsh, T. W. Smith and R. A. Kelly, *American Journal of Physiology-Heart and Circulatory Physiology*, 1994, **266**, H341–H349.
11 R. Balint, N. J. Cassidy and S. H. Cartmell, *Tissue Engineering Part B: Reviews*, 2012, **19**, 48–57.
12 L. L. Y. Chiu, R. K. Iyer, J.-P. King and M. Radisic, *Tissue Engineering Part A*, 2011, **17**, 1465–1477.
13 N. Tandon, A. Marsano, R. Maidhof, L. Wan, H. Park and G. Vunjak-Novakovic, *Journal of Tissue Engineering and Regenerative Medicine*, 2011, **5**, e115–e125.
14 K. Ronaldson-Bouchard, K. Yeager, D. Teles, T. Chen, S. Ma, L. Song, K. Morikawa, H. M. Wobma, A. Vasciaveo, E. C. Ruiz, M. Yazawa and G. Vunjak-Novakovic, *Nat Protoc*, 2019, **14**, 2781–2817.
15 X. Sun and S. S. Nunes, *Methods*, 2016, **101**, 21–26.
16 N. Tandon, A. Marsano, R. Maidhof, L. Wan, H. Park and G. Vunjak-novakovic, 2011, 115–125.
17 D. J. Dosdall, V. G. Fast and R. E. Ideker, *Annual Review of Biomedical Engineering*, 2010, **12**, 233–258.
18 P. X. de Oliveira, R. A. Bassani and J. W. M. Bassani*, *IEEE Transactions on Biomedical Engineering*, 2008, **55**, 2635–2642.
19 D. R. Merrill, M. Bikson and J. G. R. Jefferys, *Journal of Neuroscience Methods*, 2005, **141**, 171–198.
20 B. Cetin and D. Li, *Electrophoresis*, 2008, **29**, 994–1005.
21 C. Huh and M. H. Kim, *Experimental Thermal and Fluid Science*, 2006, **30**, 775–784.
22 F. Lehmann-Horn and K. Jurkat-Rott, *Physiological Reviews*, 1999, **79**, 1317–1372.
23 J. Cowgill and B. Chanda, *J. Gen. Physiol.*, 2019, **151**, 1163–1172.
24 W. A. Catterall, *J. Physiol.*, 2012, **590**, 2577–2589.
25 W. Zhu, Z. Varga and J. R. Silva, *Prog. Biophys. Mol. Biol.*, 2016, **120**, 3–17.
26 F. A. Ortega, E. Grandi, T. Krogh-Madsen and D. J. Christini, *Front Physiol*, 2017, **8**, 1099.
27 P. Imbrici, O. Nicolotti, F. Leonetti, D. Conte and A. Liantonio, in *Computational Toxicology*, Springer, 2018, pp. 313–326.
28 H. Huang, M. K. Pugsley, B. Fermini, M. J. Curtis, J. Koerner, M. Accardi and S. Authier, *J. Pharmacol. Toxicol. Methods*, 2017, **87**, 11–23.
29 A. Obergrussberger, S. Stölzle-Feix, N. Becker, A. Brüggemann, N. Fertig and C. Möller, *Channels*, 2015, **9**, 367–375.
30 C. Möller and H. Witchel, *Front. Pharmacol.*, 2011, **2**, 73.
31 T. Wang, X. Chen, J. Yu, Q. Du, J. Zhu, M. Yang, H. Wu, M. Wang and Y. Zhu, *Am. J. Chin. Med.*, 2018, **46**, 1825–1840.
32 Y. Haraguchi, A. Ohtsuki, T. Oka and T. Shimizu, *BMC Pharmacol. Toxicol.*, 2015, **16**, 39.
33 X. Li, R. Zhang, B. Zhao, C. Lossin and Z. Cao, *Arch. Toxicol.*, 2016, **90**, 1803–1816.
34 L. Ewart, M. Aylott, M. Deurinck, M. Engwall, D. J. Gallacher, H. Geys, P. Jarvis, H. Ju, D. Leishman, L. Leong, N. McMahon, A. Mead, P. Milliken, W. Suter, A. Teisman, K. Van Ammel, H. M. Vargas, R. Wallis and J. P. Valentin, *Toxicol. Sci.*, 2014, **142**, 427–435
35 M. Kim, M. Jia and T. Kim, *Analyst*, 2013, **138**, 1370–1378.
36 S. H. Ko, Y. A. Song, S. J. Kim, M. Kim, J. Han and K. H. Kang, *Lab on a Chip*, 2012, **12**, 4472–4482.
37 S. J. Kim, Y. A. Song and J. Han, *Chemical Society Reviews*, 2010, **39**, 912–922.
38 Z. Slouka, S. Senapati and H.-C. Chang, *Annual Review of Analytical Chemistry*, 2014, **7**, 317–335.
39 L.-J. Cheng and H.-C. Chang, *Lab Chip*, 2014, **14**, 979.
40 S. Marczak, K. Richards, Z. Ramshani, E. Smith, S. Senapati, R. Hill, D. B. Go and H.-C. Chang, *Electrophoresis*, 2018, **39**, 2029–2038.
41 C. Zhang, G. Sun, S. Senapati and H.-C. Chang, *Lab on a Chip*, 2019, **19**, 3853–3861.
42 J. Fu, J. Gao, R. Pi and P. Liu, *Cytotechnology*, 2005, **49**, 109–116.
43 S. Senapati, Z. Slouka, S. S. Shah, S. K. Behura, Z. Shi, M. S. Stack, D. W. Severson and H.-C. Chang, *Biosensors and Bioelectronics*, 2014, **60**, 92–100.
44 L. Sala, B. J. van Meer, L. G. J. Tertoolen, J. Bakkers, M. Bellin, R. P. Davis, C. Denning, M. A. E. Dieben, T. Eschenhagen, E. Giacomelli, C. Grandela, A. Hansen, E. R. Holman, M. R. M. Jongbloed, S. M. Kamel, C. D. Koopman, Q. Lachaud, I. Mannhardt, M. P. H. Mol, D. Mosqueira, V. V. Orlova, R. Passier, M. C. Ribeiro, U. Saleem, G. L. Smith, F. L. Burton and C. L. Mummery, *Circ Res*, , DOI:10.1161/CIRCRESAHA.117.312067.
45 A. Golberg and B. Rubinsky, *Technol Cancer Res Treat*, 2010, **9**, 423–430.
46 T. Hayakawa, T. Kunihiro, T. Ando, S. Kobayashi, E. Matsui, H. Yada, Y. Kanda, J. Kurokawa and T. Furukawa, *Journal of Molecular and Cellular Cardiology*, 2014, **77**, 178–191.
47 D. Lastochkin, R. Zhou, P. Wang, Y. Ben and H.-C. Chang, *Journal of Applied Physics*, 2004, **96**, 1730–1733.
48 O. Scheel, S. Frech, B. Amuzescu, J. Eisfeld, K.-H. Lin and T. Knott, *ASSAY and Drug Development Technologies*, 2014, **12**, 457–469.
49 M. Bébarová, *Gen. Physiol. Biophys*, 2012, **31**, 131–140.
50 R. A. Bouchard, R. B. Clark and W. R. Giles, *Circulation Research*, 1995, **76**, 790–801.

51 F. Brette, G. Luxan, C. Cros, H. Dixey, C. Wilson and H. A. Shiels, *Biochemical and Biophysical Research Communications*, 2008, **374**, 143–146.
52 B. M. Heath and D. A. Terrar, *The Journal of Physiology*, 2000, **522**, 391–402.
53 O. N. Osipenko, A. Mark Evans and A. M. Gurney, *British Journal of Pharmacology*, 1997, **120**, 1461–1470.
54 F. Hua, D. C. Johns and R. F. Gilmour, *American Journal of Physiology-Heart and Circulatory Physiology*, 2004, **286**, H2342–H2351.
55 X. Li, L. Shen, Z. Fang, X. Zou, Y. He, F. Zhang and C. Zhang, *Scientific reports*, 2017, **7**, 1–14.
56 H. Y. Zhongju, L. Zongming and I. S. Cohen, *Pflügers Archiv*, 2004, **447**, 392–400.
57 M. Biel, A. Schneider and C. Wahl, *Trends in cardiovascular medicine*, 2002, **12**, 206–213.
58 X. Yu, X. Chen, P. Zhou, L. Yao, T. Liu, B. Zhang, Y. Li, H. Zheng, L. Zheng, C. X. Zhang, I. Bruce, J. Ge, S. Wang, Z. Hu, H. Yu, Z. Zhou, X. Yu, C. X-w, P. Zhou, L. Yao, T. Liu, B. Zhang, Y. Li, Z. L-h, Z. Cx, I. Bruce, G. J-b, W. S-q and H. Z-a, *American Journal of Physiology-Cell Physiology*, 2007, **292**, 1147–1155.
59 F. Cerignoli, D. Charlot, R. Whittaker, R. Ingermanson, P. Gehalot, A. Savchenko, D. J. Gallacher, R. Towart, J. H. Price, P. M. McDonough and M. Mercola, *J. Pharmacol. Toxicol. Methods*, 2012, **66**, 246–256.
60 Y. Chang, C. N. Broyles, F. A. Brook, M. J. Davies, C. W. Turtle, T. Nagai and M. J. Daniels, *PLoS ONE*, 2017, **12**, e0174181
61 A. Chen, E. Lee, R. Tu, K. Santiago, A. Grosberg, C. Fowlkes and M. Khine, *Biomaterials*, 2014, **35**, 675–6839
62 A. Alassaf, G. Tansik, V. Mayo, L. Wubker, D. Carbonero and A. Agarwal, *Analyst*, 2020, **145**, 139–149.
63 M. L. McCain, A. Agarwal, H. W. Nesmith, A. P. Nesmith and K. K. Parker, *Biomaterials*, 2014, **35**, 5462–5471.
64 S. P. Sheehy, A. Grosberg, P. Qin, D. J. Behm, J. P. Ferrier, M. A. Eagleson, A. P. Nesmith, D. Krull, J. G. Falls, P. H. Campbell, M. L. McCain, R. N. Willette, E. Hu and K. K. Parker, *Exp. Biol. Med.*, 2017, **242**, 1643–1656.
65 A. Korolj, E. Y. Wang, R. A. Civitarese and M. Radisic, *Clin. Sci.*, 2017, **131**, 1393–1404.
66 B. Liau, N. Christoforou, K. W. Leong and N. Bursac, *Biomaterials*, 2011, **32**, 9180–9187.
67 A. P. Petersen, D. M. Lyra-Leite, N. R. Ariyasinghe, N. Cho, C. M. Goodwin, J. Y. Kim and M. L. McCain, *Cell. Mol. Bioeng.*, 2018, **11**, 337–352.
68 D. M. Lyra-Leite, A. M. Andres, A. P. Petersen, N. R. Ariyasinghe, N. Cho, J. A. Lee, R. A. Gottlieb and M. L. McCain, *Am. J. Physiol. - Hear. Circ. Physiol.*, 2017, **313**, H757–H767.
69 R. R. Besser, M. Ishahak, V. Mayo, D. Carbonero, I. Claure and A. Agarwal, *Theranostics*, 2018, **8**, 124–140.
70 U. I. Can, N. Nagarajan, D. C. Vural and P. Zorlutuna, *Adv. Biosyst.*, 2017, **1**, 1600035.
71 A. C. Zeigler, W. J. Richardson, J. W. Holmes and J. J. Saucerman, *J. Mol. Cell. Cardiol.*, 2016, **94**, 72–81.
72 K. Fountoulaki and N. Dagres, *Card. Fail. Rev.*, 2015, **1**, 64.
73 J. Zhang, R. Tao, K. F. Campbell, J. L. Carvalho, E. C. Ruiz, G. C. Kim, E. G. Schmuck, A. N. Raval, A. M. da Rocha, T. J. Herron, J. Jalife, J. A. Thomson and T. J. Kamp, *Nat. Commun.*, 2019, **10**, 1–15.
74 K. Ronaldson-Bouchard, S. P. Ma, K. Yeager, T. Chen, L. Song, D. Sirabella, K. Morikawa, D. Teles, M. Yazawa and G. Vunjak-Novakovic, *Nature*, 2018, **556**, 239–243.
75 F. Weinberger, I. Mannhardt and T. Eschenhagen, *Circ. Res.*, 2017, **120**, 1487–1500.
76 X. Yang, L. Pabon and C. E. Murry, *Circ. Res.*, 2014, **114**, 511–523.
77 S. Kadota and Y. Shiba, *Curr Cardiol Rep*, 2019, **21**, 73.
78 Y. Jiang, P. Park, S.-M. Hong and K. Ban, *Mol. Cells*, 2018, **41**, 613–621.
79 G. Buzsáki, C. A. Anastassiou and C. Koch, *Nature Reviews Neuroscience*, 2012, **13**, 407–420.
80 K.-S. Han, C. Guo, C. H. Chen, L. Witter, T. Osorno and W. G. Regehr, *Neuron*, 2018, **100**, 564-578.